

Joint Target and Ionosphere Parameter Estimation in Over-the-Horizon Radar

Ammar Ahmed, *Member, IEEE*, Yimin D. Zhang, *Fellow, IEEE*, and Braham Himed, *Fellow, IEEE*

Abstract—Target localization, especially the estimation of target altitude, is a challenging task in over-the-horizon radar (OTHR) because of the narrow signal bandwidth as well as the complexity and uncertainty involved in the ionosphere conditions. This task becomes further complicated when the height of the ionosphere layer varies over time. Therefore, it is important to jointly estimate the instantaneous height of the ionosphere and the target altitude as well as other motion parameters. In this paper, we achieve these objectives by analyzing the Doppler frequencies of the target local-multipath signals and the clutter. We reveal that the change of the ionosphere height can either enhance or deteriorate the performance of target parameter estimation depending on its direction of motion relative to the target's motion profile. In addition, it is found that the received target and clutter Doppler signatures follow the chirp signal profile at the OTHR receiver. Based on these observations, we develop a general framework that achieves joint target and ionosphere parameter estimation and accounts for the velocity and accelerations of both target and ionosphere layer. Unlike existing time-frequency-based strategies for target localization and tracking in OTHR where the Doppler signatures only directly determine target vertical velocity and the target altitude is estimated indirectly, the proposed model enables direct estimation of target altitude and ionosphere parameters. The parameter estimation problem in the proposed strategy is analytically derived and the effectiveness is verified using extensive simulation results.

Index Terms—Doppler signature, dynamic ionosphere, over-the-horizon radar, target geo-location, time-frequency analysis, fractional Fourier transform.

I. INTRODUCTION

SKY-WAVE over-the-horizon radar (OTHR) is designed to detect and track non-line-of-sight targets which are far beyond the earth horizon [1]–[4]. Unlike conventional line-of-sight radar systems which use wide-band signals to provide accurate target localization and tracking, sky-wave OTHR systems enable long-range surveillance by exploiting the ionospheric reflections of narrow-band signals whose frequency

The work of A. Ahmed and Y. D. Zhang is supported in part by a subcontract with Matrix Research, Inc. for research sponsored by the Air Force Research Laboratory under contract FA8650-14-D-1722. The work of Y. D. Zhang is also supported in part by a contract with Altamira Technologies Corp. for research sponsored by the Air Force Research Laboratory under Contract FA8650-18-C-1055.

A. Ahmed was with the Department of Electrical and Computer Engineering, Temple University, Philadelphia, PA 19122, USA. He is currently with Aptiv, Agoura Hills, CA 91301 (e-mail: ammar.ahmed@temple.edu).

Y. D. Zhang is with the Department of Electrical and Computer Engineering, Temple University, Philadelphia, PA 19122, USA (e-mail: ydzhang@temple.edu).

B. Himed is with the Distributed RF Sensing Branch, Air Force Research Laboratory, AFRL/RYSM, Dayton, OH 45433, USA (e-mail: braham.himed@us.af.mil).

and bandwidth must be properly chosen depending on the dynamic ionospheric conditions. This fact, together with the complexity and uncertainty of the time-varying ionospheric conditions, makes accurate target geo-location, especially the estimation of target altitude, extremely challenging. Significant research efforts have been dedicated to the target localization, tracking, and other associated problems in OTHR operations [5]–[9].

Target altitude information is particularly valuable for classification and perception. Direct estimation of target altitude is difficult due to several reasons, including the low range resolution associated with the narrowband radar signal and the inaccuracy in the estimated ionosphere parameters. Significant efforts have been dedicated to estimate target altitude in OTHR [10]–[17]. In [11], the authors obtained a matched-field estimate of aircraft altitude by employing multiple OTHR dwells and the altitude-dependent structure of the local multipath rays resulting from reflections local to the aircraft. This work was further extended in [12] where the altitude and altitude-rate were jointly estimated by investigating the local multipath Doppler frequencies for the case of constant altitude-rate. A state-space model-based generalized altitude estimation approach was presented in [13] where the effects of random ionospheric and target motions, that degrade the dwell-to-dwell predictability of target returns, were investigated. In [14], the authors estimate instantaneous target altitude by exploiting time-frequency signal analysis of the time-varying local multipath Doppler signatures with the initial target state being estimated using the maximum a-posteriori criterion. Target altitude estimation by exploiting two-dimensional MIMO radar using maximum likelihood estimation was discussed in [15]. An interesting experimental study of target altitude estimation by exploiting local multipath propagation model was reported in [16].

In order to achieve accurate target altitude estimation in such challenging situations, the local multipath model (also referred to as the micro-multipath model) developed in [6], [14] is considered to be effective. According to this model, the received OTHR signals consist of signal components reflected through the direct path (i.e., by an ionosphere layer) and those through the local multipath (i.e., further reflected by the specular ground/ocean surface). The specular reflection model generally applies to sea surface and when the ground surface has a low roughness. Therefore, the received OTHR signals contain signal components propagated through different paths which possess distinct Doppler signatures. Resolution of such multipath Doppler signatures through sophisticated time-frequency analysis reveals valuable information about the

target elevation velocity and enables enhanced target localization and tracking [6], [14], [17]–[20]. Existing research work in this research direction generally assumes that the target experiences a maneuvering pattern involving the elevation motion. In such a scenario, the target elevation velocity is considered as the primary source to generate a detectable frequency difference between the Doppler signatures of the OTHR signals received through different propagation paths. On the other hand, a target usually flies at a constant altitude during most of the time. In this case, the target does not yield sufficient Doppler difference to enable reliable resolution and detection of each signal component. Therefore, it is of great importance to analyze and resolve the Doppler signatures of the multi-component OTHR signals and achieve accurate target localization and tracking capability when the target flies without changing its altitude. In practice, the ionospheric conditions are continuously monitored using ionosondes but the results are subject to delays and inaccuracies [21]. Therefore, it is important to track the ionospheric parameters, along with the target motion parameters. On the other hand, the case where the velocities of the target and ionosphere vary, the estimation of target and ionosphere parameters becomes more complicated and challenging.

The problem of joint estimation of target and ionosphere parameters using their likelihood functions is discussed in [9]. Note that [9] only considers the target range, whereas the target altitude estimation, which is the main motivation of our work, is not considered. In addition, even under the condition of unchanged ionosphere height and target velocity over the processing time, as assumed in [9], real-time estimation of the parameters that characterize the statistical model of the ionosphere is not necessarily feasible because the time variations of the ionosphere are highly random and depend on several factors such as time of the day and month, penetration from high to low magnetic latitudes, and disturbance winds dynamo action [21]. Any deviation of the assumed statistical model and parameters from the actual conditions would yield degradation in the estimation accuracy of the target and ionosphere parameters.

In this paper, we perform joint estimation of target and ionosphere parameters using time-frequency-based methods, and the target is assumed to experience a constant acceleration without changing its altitude. The target and ionosphere motion parameters are estimated by exploiting the observed data. Contrary to existing work [9], we do not utilize the statistical behavior of the ionosphere motion. More specifically, we achieve accurate parameter estimation by resolving the Doppler signatures of the received signal components and extracting their parameters. We reveal that the Doppler signatures corresponding to different local multipath components are resolvable and the feasible conditions are discussed.

To provide insightful observations, we consider a flat-earth model which is an approximation of the earth curvature model but enables us to analytically study the relationship between the Doppler signatures and various parameters of interest [22]. A comparative study of the multipath Doppler signatures corresponding to the earth curvature model and the flat-earth model is provided in [23]. We derive analytical formulations

of the average Doppler and difference Doppler frequencies with approximations held under the practical assumption that the target range is much larger than the ionosphere height and the target altitude. The accuracy of the results are examined using extensive numerical simulations that are held without using these approximations related to the range. Mathematical analysis show that the target Doppler signatures can be modeled as parallel chirp signals (i.e., linear frequency modulated signals) with Doppler frequency varying linearly with time. The frequency difference between the Doppler signatures of different local multipath components is proportional to the carrier frequency, ionosphere height, target altitude, and target horizontal velocity, but is inversely proportional to the square of the target range.

We further consider the effect of velocity and acceleration of the height of the ionosphere layer. Ionospheric layers experience different patterns of altitude variations. For example, the E-layer is relatively stable, whereas the F-layers show more rapid and dynamic variations. Time variation in the ionosphere height acts as another source that changes the Doppler signatures of the targets and induces additional frequency difference between the multipath Doppler signatures. We show that, depending on the relative directions of the target motion and the ionosphere height variation, their respective contributions to the Doppler frequency difference may be constructive or destructive, which respectively make the detection and resolution of Doppler signatures easier or more difficult.

We verify our analysis with numerical simulations in different situations with and without variation in the ionosphere and target velocity. The time-varying Doppler signatures are visualized using the spectrogram, whereas the fractional Fourier transform (FrFT) is exploited to detect the chirp rate as well as the centroid frequency. The obtained chirp parameters are then used to estimate the parameters of the target and the ionosphere, including their height, velocity and acceleration.

II. SIGNAL MODEL

A. Multipath Propagation Geometry

Consider an OTHR system characterized using a flat-earth ionosphere model, as shown in Fig. 1. A point-like isotropic target is assumed to be moving at a constant but unknown altitude h above the ground or sea surface [14]. In Fig. 1, the propagation paths and the target below the ionosphere layer are actual ones, whereas those above the ionosphere layer are virtual ones that illustrate the mirrored images of the actual propagation paths and targets through the ionosphere layer and ground/sea reflections.

It is observed in Fig. 1 that the specular reflection from the ground or sea surface results in different transmit and receive paths whose combinations can be represented in the form of three distinct components. The first component reflects the signals transmitted and received along path I. For the second component, both the transmitted and received signals follow the propagation along path II. The third component comprises two propagation paths, one emitting along path I and returning along path II whereas the other emitting along path II and returning along path I.

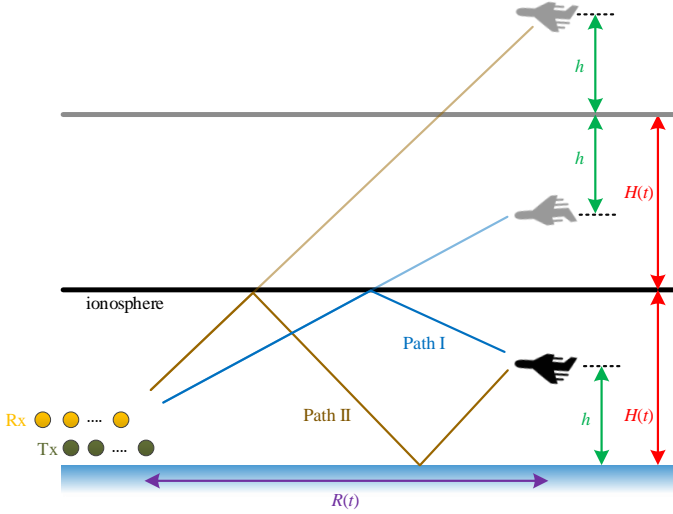


Fig. 1: Flat-earth model of local multipath propagation in an OTHR system.

Consider a coherent processing interval (CPI) of $0 \leq t \leq T$, and denote $H(t)$ as the time-varying height of the ionosphere layer, where a *coarse* estimate of its initial height, $H(0) = H_0$, is assumed to be known from ionosonde monitoring. As we can see in the sequel, the detection and resolution of the target multipath Doppler signatures are not sensitive to the initial height of the ionosphere layer.

From Fig. 1, the one-way slant ranges $l_1(t)$ and $l_2(t)$ of path I and path II are obtained in terms of the ground range $R(t)$, the ionosphere height $H(t)$, and the target altitude h , as

$$\begin{aligned} l_1(t) &= [R^2(t) + (2H(t) - h)^2]^{1/2}, \\ l_2(t) &= [R^2(t) + (2H(t) + h)^2]^{1/2}. \end{aligned} \quad (1)$$

The slant ranges of the three round-trip paths (path 1: $[l_1(t), l_1(t)]$, path 2: $[l_2(t), l_2(t)]$, and path 3: $[l_1(t), l_2(t)]$ or $[l_2, l_1]$) are expressed as

$$L_1(t) = 2l_1(t), \quad L_2(t) = 2l_2(t), \quad L_3(t) = l_1(t) + l_2(t). \quad (2)$$

In this paper, we consider a general and challenging situation where the target and ionosphere layer have time-varying velocities and their respective accelerations are considered to be constant. This assumption is reasonable because we are processing the data over a short time period.

For notational simplicity, we omit the explicit notation of (t) in the sequel.

B. Doppler Signatures

The Doppler signatures corresponding to the three round-trip paths can be obtained as

$$f_{D,i} = -\frac{f_c}{c} \dot{L}_i, \quad i = 1, 2, 3, \quad (3)$$

where the path lengths L_i are given in Eq. (2), and $\dot{L}_i = dL_i/dt$ represents the derivative of L_i with respect to time. In addition, f_c is the carrier frequency of the transmitted signal, and c is the speed of electromagnetic wave in free space.

In order to provide insightful observations of the relationship between the Doppler frequencies and the target parameters, we approximate the one-way slant ranges in Eq. (1) using the first-order Taylor series expansion. Assuming $R \gg H \gg h$ holds in practice, we can write

$$\begin{aligned} l_1 &\approx R + \frac{(2H - h)^2}{2R} = R + \frac{4H^2 - 4Hh + h^2}{2R} \\ &\approx R + \frac{2H^2 - 2Hh}{R}, \\ l_2 &\approx R + \frac{(2H + h)^2}{2R} = R + \frac{4H^2 + 4Hh + h^2}{2R} \\ &\approx R + \frac{2H^2 + 2Hh}{R}. \end{aligned} \quad (4)$$

Taking the derivative of the above one-way slant ranges with respect to time, we obtain

$$\begin{aligned} \dot{l}_1 &\approx \dot{R} + \frac{2H}{R^2} (2\dot{H}R - H\dot{R}) - \frac{2h}{R^2} (\dot{H}R - H\dot{R}), \\ \dot{l}_2 &\approx \dot{R} + \frac{2H}{R^2} (2\dot{H}R - H\dot{R}) + \frac{2h}{R^2} (\dot{H}R - H\dot{R}). \end{aligned} \quad (5)$$

We can express the time derivatives of the range and the ionosphere height in terms of their initial velocity and acceleration as

$$\dot{R} = \dot{R}_0 + \ddot{R}t, \quad \dot{H} = \dot{H}_0 + \ddot{H}t, \quad (6)$$

where \dot{R}_0 denotes the horizontal velocity of the target, \dot{H}_0 is the initial vertical velocity of the ionosphere, whereas \ddot{R} and \ddot{H} denote their respective accelerations which are assumed constant during the entire processing time. It is noted that, for both the target and the ionosphere layer, positive velocities are defined for the motion when the value of range and ionosphere height increases. Substituting Eq. (6) in Eq. (5) yields

$$\begin{aligned} \dot{l}_1 &\approx (\dot{R}_0 + \ddot{R}t) + \frac{2H}{R^2} [2(\dot{H}_0 + \ddot{H}t)R - H(\dot{R}_0 + \ddot{R}t)] \\ &\quad - \frac{2h}{R^2} [(\dot{H}_0 + \ddot{H}t)R - H(\dot{R}_0 + \ddot{R}t)], \\ \dot{l}_2 &\approx (\dot{R}_0 + \ddot{R}t) + \frac{2H}{R^2} [2(\dot{H}_0 + \ddot{H}t)R - H(\dot{R}_0 + \ddot{R}t)] \\ &\quad + \frac{2h}{R^2} [(\dot{H}_0 + \ddot{H}t)R - H(\dot{R}_0 + \ddot{R}t)]. \end{aligned} \quad (7)$$

The Doppler frequencies of the received OTHR signal due to the three different paths are then respectively given as

$$\begin{aligned} f_{D,1} &= \bar{f}_D + \Delta f_D, \\ f_{D,2} &= \bar{f}_D - \Delta f_D, \\ f_{D,3} &= \bar{f}_D, \end{aligned} \quad (8)$$

where

$$\begin{aligned} \bar{f}_D &= -\frac{f_c}{c} \frac{d(l_1 + l_2)}{dt} \approx -\frac{2f_c}{c} (\dot{R}_0 + \ddot{R}t) \\ &\quad - \frac{4f_c H}{cR^2} [2(\dot{H}_0 + \ddot{H}t)R - H(\dot{R}_0 + \ddot{R}t)], \end{aligned} \quad (9a)$$

$$\begin{aligned} \Delta f_D &= -\frac{f_c}{c} \frac{d(l_1 - l_2)}{dt} \\ &\approx \frac{4f_c h}{cR^2} [(\dot{H}_0 + \ddot{H}t)R - H(\dot{R}_0 + \ddot{R}t)]. \end{aligned} \quad (9b)$$

It is clear from Eqs. (8) and (9) that the target and ionosphere parameters for path 1 and path 2 symmetrically wrap around the Doppler signatures generated due to path 3. The average Doppler component, \bar{f}_D , is shared by all three propagation paths, whereas Δf_D characterizes the symmetrical difference of the Doppler frequencies between these different paths. Note that both \bar{f}_D and Δf_D are functions of \dot{R} and \ddot{H} . If the three Doppler components are resolvable from the received data, they would enable joint parameter estimation of the target and the ionosphere layer by analyzing their respective Doppler signatures. It is noted that Eqs. (8) and (9) are also valid for the Doppler signatures generated due to clutter by letting $h = 0$, $\dot{R}_0 = 0$, and $\ddot{R} = 0$.

From Eq. (9b), note that the relative direction of the ionosphere motion as well as the target can either increase or decrease the Doppler separation Δf_D . Since it is difficult to resolve the closely-spaced frequency components, the relative motion of ionosphere and target can have a constructive or destructive effect on the frequency resolution capability of OTHR.

The required CPI depends on the Doppler difference between local multipath signal components. For the parameters considered in this paper, the Doppler difference between local multipath signal components is generally on the order of a fraction of a Hz. We know that the required observation time T to resolve any two closely separated frequencies with separation of Δf is given by $T \propto 1/\Delta f$. Therefore, a large CPI is typically required to resolve a small frequency separation between the three local multipath Doppler components generated by the target. Such a large CPI is supported by the current state-of-the-art [6], [19], [24], [25].

III. STABLE IONOSPHERE LAYER CASE

In this section, we consider the case where the altitude of the ionosphere layer does not change over time, whereas the target moves towards or away from the radar with a constant acceleration. In this case, $\dot{H}_0 = 0$, $\ddot{H} = 0$, and $H = H_0$. We first analyze the effect of the target motion on the estimated Doppler frequencies, and then develop a framework for the estimation of target height and motion parameters. The analysis and parameter estimation for the case of time-varying ionosphere height are provided in Section IV.

A. Doppler Signature Analysis

For the case of a constant ionosphere layer height, by taking $\dot{H}_0 = 0$ and $\ddot{H} = 0$ into account, Eq. (9) becomes

$$\bar{f}_D \approx -\frac{2f_c}{c} \left(1 - \frac{2}{R^2} H^2\right) (\dot{R}_0 + \ddot{R}t), \quad (10a)$$

$$\Delta f_D \approx -\frac{4f_c}{cR^2} Hh (\dot{R}_0 + \ddot{R}t). \quad (10b)$$

That is, the received signal contains three frequency components expressed in Eq. (8) where \bar{f}_D and Δf_D are given by Eq. (10).

Proposition 1: For a stable ionosphere layer with a constant height, the received signal due to horizontal motion of the

target with a constant acceleration can be approximately represented as the sum of three chirp signals.

Proof: First, we take the time derivative of Eq. (10) as

$$\dot{\bar{f}}_D \approx -\frac{2f_c}{c} \left[\left(1 - \frac{2}{R^2} H^2\right) \ddot{R} + \frac{4(\dot{R}_0 + \ddot{R}t)^2}{R^3} H^2 \right], \quad (11a)$$

$$\Delta \dot{f}_D \approx -\frac{4f_c}{c} Hh \left(\frac{\ddot{R}}{R^2} - \frac{2(\dot{R}_0 + \ddot{R}t)^2}{R^3} \right). \quad (11b)$$

Since the traveling distance of the target during the processing time is much smaller than the target range, we can treat R as a constant. In this case, we can approximate Eq. (11) as

$$\dot{\bar{f}}_D \approx -\frac{2f_c}{c} \left(1 - \frac{2}{R^2} H^2\right) \ddot{R}, \quad (12a)$$

$$\Delta \dot{f}_D \approx -\frac{4f_c Hh}{cR^2} \ddot{R}. \quad (12b)$$

The changes in frequency for the three Doppler frequencies $f_{D,1}$, $f_{D,2}$, and $f_{D,3}$ can respectively be expressed as

$$r_{D,1} = \dot{\bar{f}}_D + \Delta \dot{f}_D \approx -\frac{2f_c}{c} \left(1 - \frac{2(H-h)H}{R^2}\right) \ddot{R}, \quad (13a)$$

$$r_{D,2} = \dot{\bar{f}}_D - \Delta \dot{f}_D \approx -\frac{2f_c}{c} \left(1 - \frac{2(H+h)H}{R^2}\right) \ddot{R}, \quad (13b)$$

$$r_{D,3} = \dot{\bar{f}}_D \approx -\frac{2f_c}{c} \left(1 - \frac{2}{R^2} H^2\right) \ddot{R}. \quad (13c)$$

It can be observed that such Doppler frequency changes are almost constant (with insignificant variations due to the change in R). Therefore, Eq. (13) shows that the received signal is the sum of three chirp signals where the chirp rates are directly proportional to the target acceleration.

B. Chirp Parameter Estimation

We exploit two methods in order to visualize the three chirp signals from the received OTHR signal $x(t)$. In the first method, we use the spectrogram of $x(t)$, which is the magnitude square of the short-time Fourier transform (STFT), expressed as [26]

$$X(t, f) = \left| \int_{-\infty}^{\infty} x(u)g(t-u) \exp(-j2\pi fu) du \right|^2, \quad (14)$$

where $g(t)$ is a window function. In this paper, the Hamming window is used. In the second method, we employ FrFT which not only enables the visualization of Doppler signatures but is also effective in estimating the parameters of the chirp signals [27]–[29]. The FrFT of the signal $x(t)$, denoted as $\mathcal{X}_\alpha(u)$, is defined as [27], [28]

$$\mathcal{X}_\alpha(u) = \int_{-\infty}^{\infty} x(t) \mathcal{K}_\alpha(t, u) dt, \quad (15)$$

where

$$\mathcal{K}_\alpha(t, u) = \begin{cases} \sqrt{\frac{1 - j \cot(\phi)}{2\pi}} e^{j \frac{u^2}{2} \cot(\phi)} \\ \times e^{j \frac{t^2}{2} \cot(\phi)} e^{-ju \csc(\phi)}, & \phi \neq k\pi, \\ \delta(t - u), & \phi = 2k\pi, \\ \delta(t + u), & \phi + \pi = 2k\pi, \end{cases}$$

and k is a non-negative integer and $\phi = \alpha\pi/2$.

We know that the received OTHR signals consist of three distinct Doppler components where each component follows the characteristics of a chirp signal. Using the received signal $x(t)$, a two-dimensional spectrogram image can be plotted with respect to frequency u and rotation angle α . Three equispaced peaks are estimated in the fractional Fourier axis using the FrFT plot. Subsequently, the maximum rotation angle α_{opt} is recorded for each frequency. Once the optimal rotation angle α_{opt} is determined, we can find the chirp rate of each respective chirp signal using the following equation [28], [29]:

$$\hat{\mu} = -\cot(\alpha_{\text{opt}}\pi/2) \frac{f_s^2}{N}, \quad (16)$$

where $\hat{\mu}$ is the estimated chirp rate of the Doppler components, f_s is the pulse repetition frequency, and N is the number of samples used for calculating the FrFT. The centroid frequency of the chirp can be found as [30]

$$f_{\text{centroid}} = \frac{f_{\text{frft}}}{\sin(\alpha_{\text{opt}}\pi/2)}, \quad (17)$$

where f_{frft} is the estimated peak frequency of the individual chirp in the fractional domain. Once three equispaced frequencies are estimated, differential component Δf can be easily calculated by taking the average of two intra-frequency spacings.

C. Target Parameter Estimation

Substituting $(\dot{R}_0 + \ddot{R}t)$ from Eq. (10a) into Eq. (10b) and isolating the target altitude, we obtain the estimated target altitude at time $t = 0$ as

$$\hat{h} = \frac{(R_0^2 - 2H^2)\Delta f_D}{2H\bar{f}_{D,0}}, \quad (18)$$

where R_0 is the initial target range and $\bar{f}_{D,0}$ denotes the estimated average Doppler component at time $t = 0$. Note that $\bar{f}_{D,t}$ can be calculated using the centroid frequency of the average Doppler component and the corresponding chirp rate, obtained using Eqs. (16) and (17) through FrFT, given as

$$\bar{f}_{D,t} = \bar{f}_{D,\text{center}} - (t - 0.5T) \dot{f}_D, \quad (19)$$

where $\bar{f}_{D,\text{center}}$ and \dot{f}_D are the estimated centroid frequency and the corresponding chirp rate of the average Doppler component, respectively. By substituting Eq. (18) into Eq. (10b), we obtain the instantaneous target velocity as

$$\dot{R} = \dot{R}_0 + \ddot{R}t = -\frac{cR_0^2 \bar{f}_{D,0}}{2f_c(R_0^2 - 2H^2)}, \quad (20)$$

Substituting $t = 0$ in (20), we obtained the estimated initial target velocity as

$$\hat{R}_0 = -\frac{cR_0^2 \bar{f}_{D,0}}{2f_c(R_0^2 - 2H^2)}. \quad (21)$$

Substituting (21) into (20) at $t = T$, we obtain

$$\hat{R} = \frac{c}{2f_c T} \frac{(R_T^2 \bar{f}_{D,T} - R_0^2 \bar{f}_{D,0})}{(R_0^2 - 2H^2)},$$

where R_T is the target range at time T . As the change in range is insignificant during the entire processing time, i.e. $R \approx R_0 \approx R_T$, we get

$$\begin{aligned} \hat{R} &\approx \frac{c}{2f_c T} \left(\frac{R_0^2}{R_0^2 - 2H^2} \right) (\bar{f}_{D,0} - \bar{f}_{D,T}) \\ &= -\frac{c}{2f_c} \left(\frac{R_0^2}{R_0^2 - 2H^2} \right) \dot{f}_D. \end{aligned} \quad (22)$$

Since $R \gg H$, an error in the ionosphere altitude information has a negligible impact on target velocity and acceleration estimation as can be observed in Eqs. (21) and (22). However, Eq. (18) shows direct dependency between the accuracy of the target altitude estimation and that of the ionosphere height information. Note that Eq. (22) is equivalent to Eq. (13c) for the estimation of the target acceleration.

IV. TIME-VARYING IONOSPHERE ALTITUDE CASE

In this section, we consider the case where the ionosphere height varies with time with a constant acceleration. Similar to the stable ionosphere layer case considered in Section III, the target is assumed to move towards or away from the radar with a constant acceleration.

A. Doppler Signature Analysis

As illustrated in Eq. (9), the variation of the ionosphere altitude, $\dot{H}_0 + \ddot{H}t$, affects both the average Doppler frequency and the difference Doppler frequency. In this case, the difference Doppler frequency is proportional to $(\dot{H}_0 + \ddot{H}t)R - H(\dot{R}_0 + \ddot{R}t)$. It is thus clear that both the motion of ionosphere and that of the target contribute to the yielding Doppler frequency, and their contributions can be either constructive

TABLE I: Key Parameters (Unless Otherwise Specified)

Parameter	Notation	Value
Initial range	R_0	2,500 km
Initial ionosphere height	H_0	350 km
Target altitude	h	20 km
Initial target velocity (horizontal)	\dot{R}_0	± 400 m/s
Initial ionosphere velocity (vertical)	\dot{H}_0	± 35 m/s
Target acceleration (horizontal)	\ddot{R}	± 3 m/s ²
Ionosphere acceleration (vertical)	\ddot{H}	± 0.5 m/s ²
Carrier frequency	f_c	16 MHz
Pulse repetition frequency	f_s	140 Hz
Signal-to-noise ratio	SNR	-15 dB
Clutter-to-noise ratio	CNR	35 dB
Coherent processing interval	T	60 s

TABLE II: SUMMARY OF ESTIMATION EQUATIONS

Estimation Parameter	Stationary Ionosphere Case	Moving Ionosphere Case
Step 1: Estimate the frequencies and the chirp rates of target and clutter Doppler signatures using FrFT		
$\mathcal{X}_\alpha(u) = \int_{-\infty}^{\infty} x(t)\mathcal{K}_\alpha(t,u)dt$, where $\mathcal{K}_\alpha(t,u) =$	$\begin{cases} \sqrt{\frac{1-j\cot(\phi)}{2\pi}} e^{j\frac{u^2}{2}\cot(\phi)} e^{j\frac{t^2}{2}\cot(\phi)} e^{-ju\csc(\phi)}, & \phi \neq k\pi, \\ \delta(t-u), & \phi = 2k\pi, \\ \delta(t+u), & \phi + \pi = 2k\pi \end{cases}$	
Step 2: Calculate ionosphere parameters		
Initial ionosphere velocity (vertical)	$\hat{H}_0 = 0$	$\hat{H}_0 = -\frac{cR_0\dot{f}_{D,0}^{\text{clutter}}}{8f_c H_0}$
Ionosphere acceleration (vertical)	$\hat{H} = 0$	$\hat{H} = -\frac{\dot{f}_{D,0}^{\text{clutter}} cR_0}{8f_c H_0}$
Step 3: Estimate target parameters		
Target initial velocity	$\hat{R}_0 = -\frac{cR_0^2\dot{f}_{D,0}}{2f_c(R_0^2 - 2H^2)}$	$\hat{R}_0 = -\frac{R_0^2}{R_0^2 - 2H_0^2} \left(\frac{c\bar{f}_{D,0}}{2f_c} + \frac{4H_0\dot{H}_0}{R_0} \right)$
Target acceleration	$\hat{R} = -\frac{c}{2f_c} \left(\frac{R_0^2}{R_0^2 - 2H_0^2} \right) \dot{f}_D$	$\hat{R} = \frac{R_0^2}{T} \left[\frac{1}{R_0^2 - 2H_0} \left(\frac{c\bar{f}_{D,0}}{2f_c} + \frac{4H_0\dot{H}_0}{R_0} \right) - \frac{1}{R_0^2 - 2H_T} \left(\frac{c\bar{f}_{D,T}}{2f_c} + \frac{4H_T\dot{H}_T}{R_0} \right) \right]$
Target altitude	$\hat{h} = \frac{(R_0^2 - 2H^2)\Delta f_D}{2H\dot{f}_D}$	$\hat{h} = \frac{\Delta f_{D,0} cR_0^2}{4f_c(\dot{H}_0 R_0 - H_0 \dot{R}_0)}$

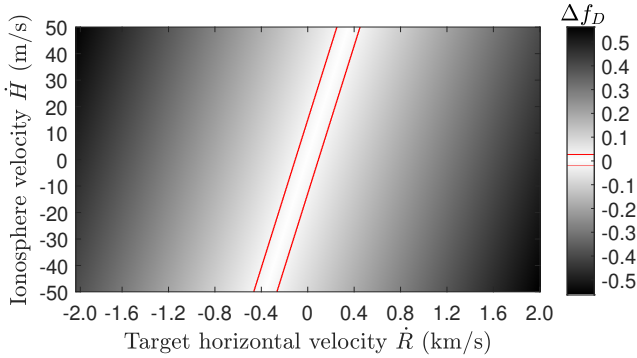


Fig. 2: The difference Doppler component Δf_D (in Hz) for different instantaneous velocities of ionosphere and target ($R = 2,500$ km, $H = 350$ km, $f_c = 16$ MHz).

or destructive, depending on the direction of their velocities. Constructive superposition of the Doppler frequencies due to the target and ionosphere motions will make the difference Doppler frequency higher for easier detection and estimation of the three Doppler signatures. On the other hand, when they are approximately in the same order of magnitude, destructive combination of their contributions will significantly reduce the difference Doppler frequency and, as a result, make it difficult to resolve the three Doppler signatures. For example, when the target is moving towards the radar (with a negative velocity) and the ionosphere is ascending (with a positive velocity), their mutual effect in Eq. (9) adds constructively, resulting in a higher value of $|\Delta f_D|$ for easier separation of the three Doppler components. On the other hand, when either of these two components changes direction, $|\Delta f_D|$ becomes smaller and the Doppler signatures of the multipath signals become more difficult to resolve due to their proximity

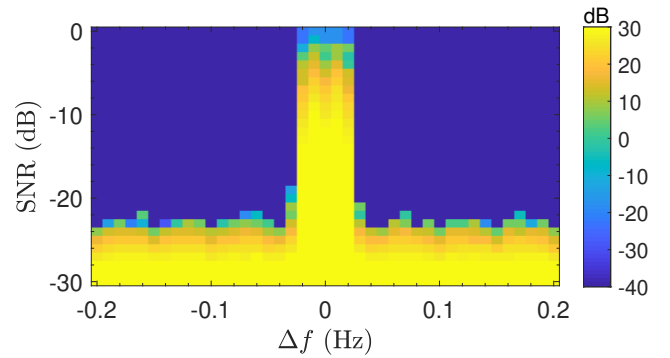


Fig. 3: RMSE of multipath Doppler frequency estimates for varying Δf and SNR ($R = 2,500$ km, $H = 350$ km, $f_c = 16$ MHz, $M = 1000$ trials).

in the frequency domain. However, considering the typical velocities of targets and the ionosphere, such challenging cases of resolving Doppler frequencies appear with a relatively low probability.

B. Ionosphere Parameter Estimation from Clutter Doppler Signature

As discussed earlier, while the OTHR system typically provides a coarse estimate of the ionosphere altitude from an ionosonde, it generally does not provide a timely and accurate update about the ionosphere velocity and instantaneous height. The velocity and acceleration of the ionosphere must be estimated. In this sub-section, we utilize the Doppler signatures of the clutter to estimate the ionosphere parameters.

To consider the clutter Doppler frequencies, we use Eq. (9) and let $\dot{R}_0 = 0$, $\ddot{R} = 0$ and $h = 0$. As such, the difference Doppler frequency $\Delta f_D^{\text{clutter}} = 0$, as there are no

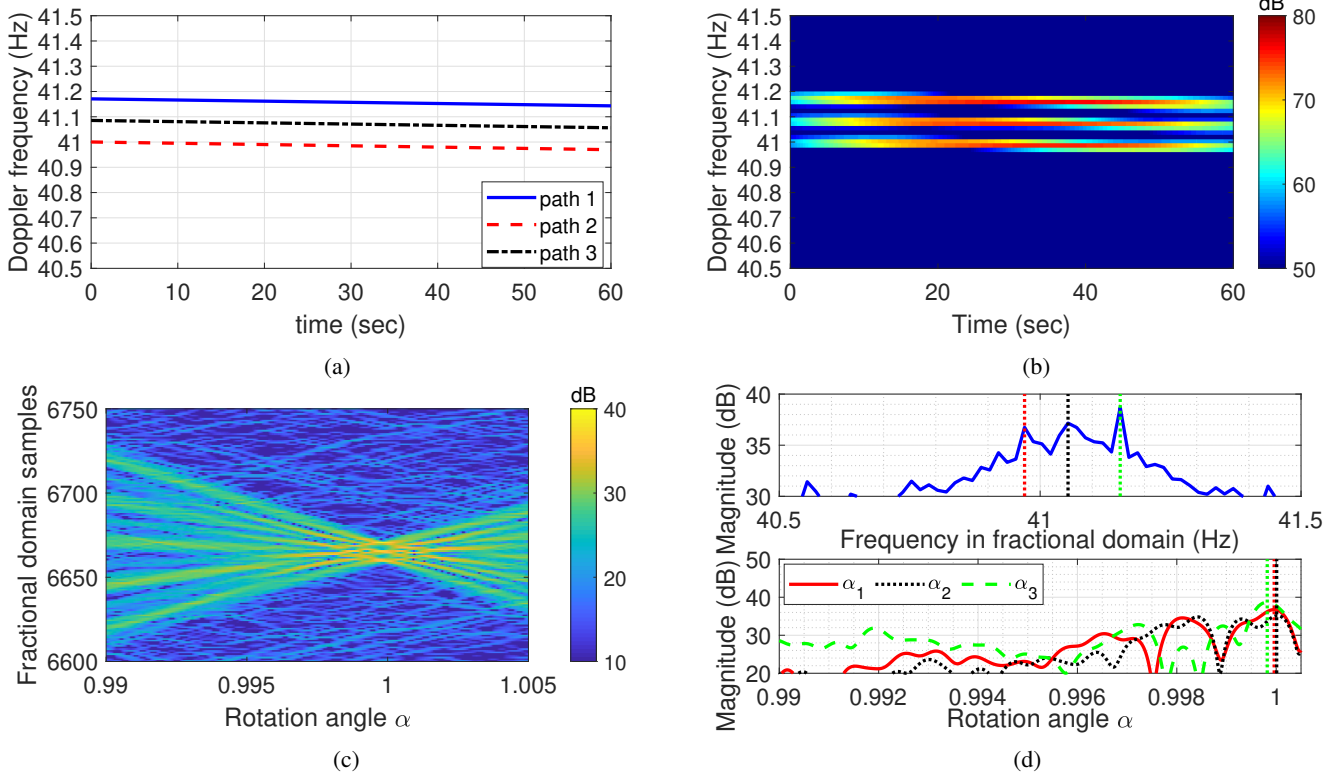


Fig. 4: Doppler signatures of local multipath signals for the case of stable ionosphere while the target is moving towards the radar at altitude $h = 20$ km with velocity $\dot{R}_0 = -400$ m/s and acceleration $\ddot{R} = 0$ m/s². (a) Simulated Doppler signature; (b) Spectrogram using a Hamming window of size 4096; (c) Fractional Fourier transform; (d) Peak detection in frequency domain and the corresponding α plotted for each of the peak frequencies. Input SNR is set at -15 dB. The target parameters estimated from this simulation are $\hat{h} = 18.81$ km, $\hat{R}_0 = -400.48$ m/s, and $\hat{\ddot{R}} = -4.6 \times 10^{-5}$ m/s².

local multipaths for the ground and sea clutter in this case. The average Doppler frequency is given by

$$\begin{aligned} \bar{f}_D^{\text{clutter}} &\approx -\frac{8f_c H}{cR} (\dot{H}_0 + \ddot{H}t) \\ &= -\frac{8f_c}{cR} \left(H_0 + \dot{H}_0 t + \frac{1}{2} \ddot{H} t^2 \right) (\dot{H}_0 + \ddot{H}t), \end{aligned} \quad (23)$$

where H_0 is the initial ionosphere altitude measured by the ionosonde. Given a coarse knowledge of the initial target range, we can use Eq. (23) with $t = 0$ to determine the initial velocity of the ionosphere as

$$\hat{H}_0 = -\frac{cR_0 \bar{f}_{D,0}^{\text{clutter}}}{8f_c H_0}. \quad (24)$$

Substituting $t = T$ in Eq. (23), we estimate the ionosphere acceleration as

$$\begin{aligned} \hat{\ddot{H}} = &-\frac{1}{2T^2} \left[(2H_0 + 3\dot{H}_0 T) \right. \\ &\left. - (2H_0 + \dot{H}_0 T) \left(1 - \frac{cR_T \bar{f}_{D,T}^{\text{clutter}}}{f_c (2H_0 + \dot{H}_0 T)^2} \right)^{1/2} \right]. \end{aligned} \quad (25)$$

In the above expression, approximations $cR_T \bar{f}_{D,T}^{\text{clutter}} T / [f_c (2H_0 + \dot{H}_0 T)^2] \ll 1$ and $R \approx R_0 \approx R_T$ are satisfied in practice. In this case, we can apply the Taylor series approximation on Eq. (25) and approximate the

ionosphere acceleration as

$$\hat{\ddot{H}} \approx -\frac{1}{T} \left[\dot{H}_0 + \frac{1}{4} \frac{cR_0 \bar{f}_{D,T}^{\text{clutter}}}{f_c (2H_0 + \dot{H}_0 T)} \right]. \quad (26)$$

Proposition 2: The clutter Doppler frequency $\bar{f}_D^{\text{clutter}}$ can be approximated by a chirp.

Proof: As we discussed previously, the effect of the range variation over the CPI can be ignored. By taking the derivative of Eq. (23) with time, we obtain

$$\dot{\bar{f}}_D^{\text{clutter}} = -\frac{8f_c}{cR} \left(H_0 \ddot{H} + \dot{H}_0^2 + 3\dot{H}_0 \ddot{H}t + \frac{3}{2} \ddot{H}^2 t^2 \right). \quad (27)$$

The effect of time-varying terms involving $\ddot{H}t$ and $\ddot{H}^2 t^2$ can be ignored. For example, for an ionosphere layer at an altitude of 350 km moving with a velocity of 35 m/s and an acceleration of 0.5 m/s² and CPI of 60 s, $3\dot{H}_0 \ddot{H}t + (3/2)\ddot{H}^2 t^2$ is only 2.55% of $H_0 \ddot{H} + \dot{H}_0^2$ and thus is insignificant. The impact becomes even smaller when a shorter CPI is considered. After ignoring these insignificant terms, Eq. (27) can be simplified as

$$\dot{\bar{f}}_D^{\text{clutter}} \approx -\frac{8f_c}{cR} (H_0 \ddot{H} + \dot{H}_0^2). \quad (28)$$

As a result, the clutter Doppler frequency can be approximated by a chirp signal whose chirp rate $\dot{\bar{f}}_D^{\text{clutter}}$ is approximately constant.

From Eq. (28), the ionosphere acceleration can be estimated

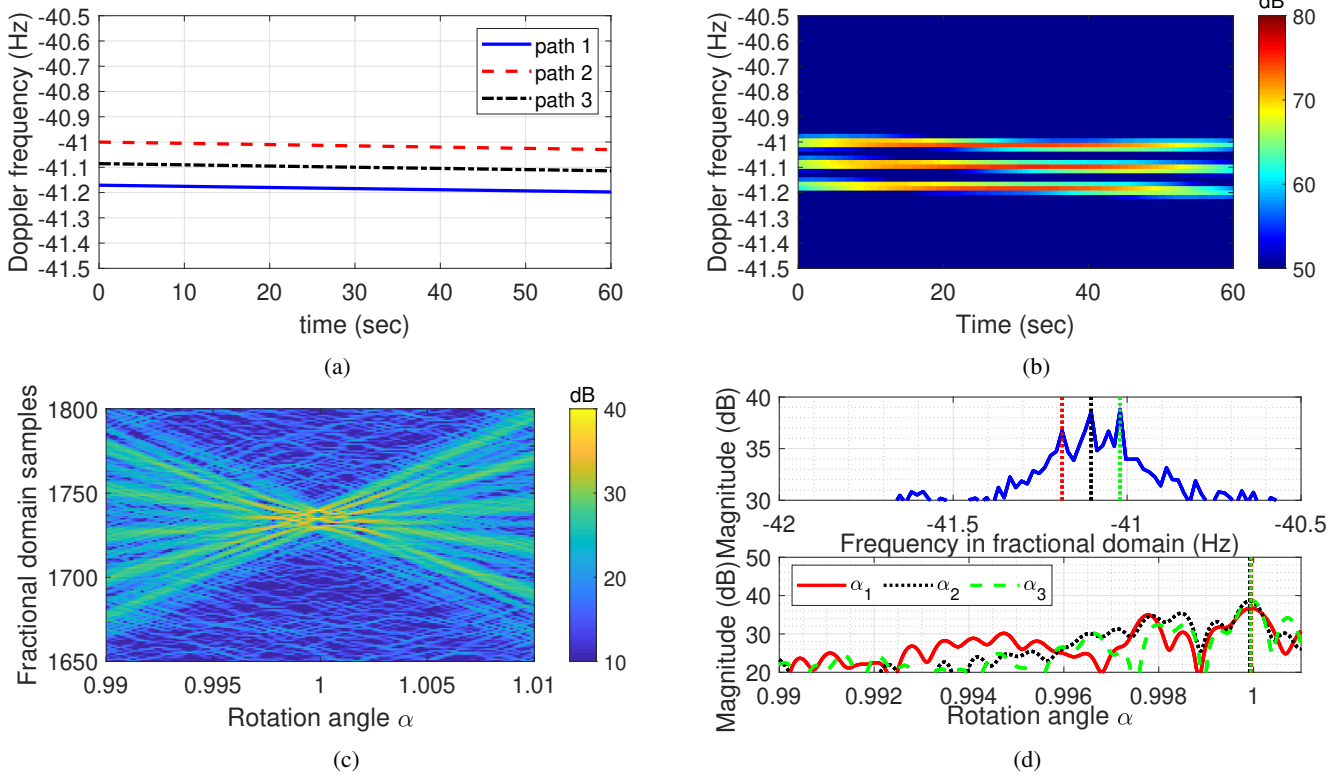


Fig. 5: Doppler signatures of local multipath signals for the case of stable ionosphere while the target is moving away from the radar at altitude $h = 20$ km with velocity $R_0 = 400$ m/s and acceleration $\ddot{R} = 0$ m/s². (a) Simulated Doppler signature; (b) Spectrogram using a Hamming window of size 4096; (c) Fractional Fourier transform; (d) Peak detection in frequency domain and the corresponding α plotted for each of the peak frequencies. Input SNR is set at -15 dB. The target parameters estimated from this simulation are $\hat{h} = 17.74$ km, $\hat{R}_0 = 401.12$ m/s, and $\hat{\ddot{R}} = 1.5 \times 10^{-5}$ m/s².

as

$$\hat{\dot{H}} = - \left(\frac{\dot{f}_D^{\text{clutter}} c R}{8 f_c H_0} + \frac{\dot{H}_0^2}{H_0} \right), \quad (29)$$

where $\dot{f}_D^{\text{clutter}}$ can be estimated as the chirp rate of the Doppler frequency through the FrFT, and \dot{H}_0^2 can be found using Eq. (24). The parameter \dot{H}_0^2/H_0 is negligible for a high value of H_0 . For example, for an ionosphere height of 350 km and ionosphere velocity of 35 m/s, $\dot{H}_0^2/H_0 = 3.5 \times 10^{-3}$ m/s². Assuming $R \approx R_0 \approx R_T$, Eq. (29) can be simplified as

$$\hat{\dot{H}} \approx - \frac{\dot{f}_D^{\text{clutter}} c R_0}{8 f_c H_0}. \quad (30)$$

C. Target Parameter Estimation

It can be observed from Eq. (9) that the ionosphere height has an impact on the observed Doppler frequencies. Therefore, the observed Doppler frequencies at the OTHR receiver contain the contributions from the target motion and the variation due to the dynamic ionosphere height. To estimate the target parameters, we utilize the ionosphere layer parameters obtained in Section IV-B, and isolate \dot{R} from Eq. (9a), and obtain the following estimate of the target velocity:

$$\dot{R} + \ddot{R}t = - \frac{R^2}{R^2 - 2H^2} \left(\frac{c \bar{f}_D}{2 f_c} + \frac{4H\dot{H}}{R} \right). \quad (31)$$

Substituting $t = 0$ in Eq. (31), we obtain the following estimation equation for range-rate

$$\hat{R}_0 = - \frac{R_0^2}{R_0^2 - 2H_0^2} \left(\frac{c \bar{f}_{D,0}}{2 f_c} + \frac{4H_0\dot{H}_0}{R_0} \right), \quad (32)$$

Eq. (31) and Eq. (32) can be used at $t = T$ while assuming $R \approx R_0 \approx R_T$, we get

$$\hat{\dot{R}} = \frac{R_0^2}{T} \left[\frac{1}{R_0^2 - 2H_0} \left(\frac{c \bar{f}_{D,0}}{2 f_c} + \frac{4H_0\dot{H}_0}{R_0} \right) - \frac{1}{R_0^2 - 2H_T} \left(\frac{c \bar{f}_{D,T}}{2 f_c} + \frac{4H_T\dot{H}_T}{R_0} \right) \right], \quad (33)$$

where the ionosphere final altitude is given by $H_T = H_0 + \dot{H}_0 T + (1/2)\ddot{H}T^2$ and the final velocity can be calculated as $\dot{H}_T = \dot{H}_0 + \ddot{H}T$, whereas $\bar{f}_{D,0}$ is the initial average Doppler frequency and can be calculated using the estimated centroid frequency and the estimated chirp rate. The target altitude h can be estimated by rearranging Eq. (9b) for $t = 0$ as

$$\hat{h} = \frac{\Delta f_{D,0} c R^2}{4 f_c (\dot{H}_0 R - H_0 \dot{R}_0)}. \quad (34)$$

Substituting the estimated \dot{R}_0 and \dot{H}_0 into Eq. (34), we

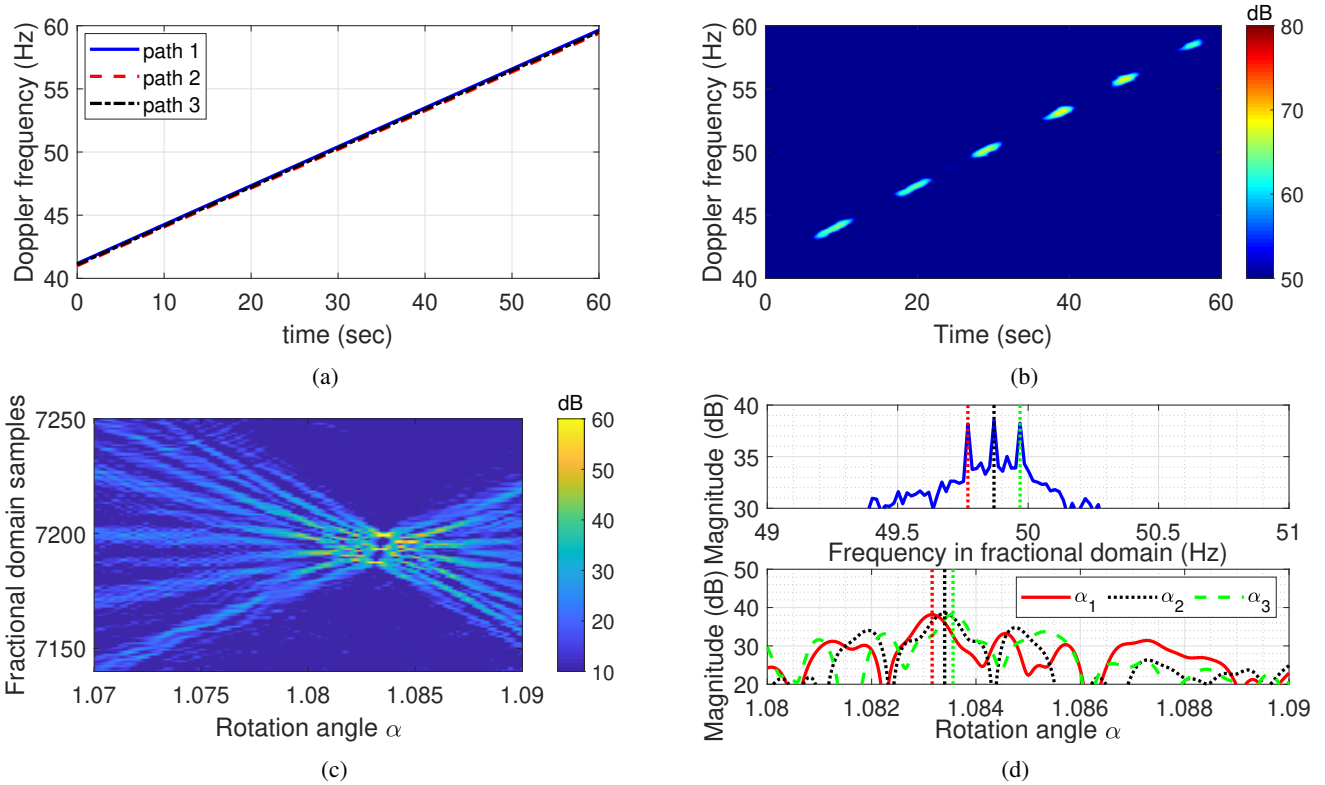


Fig. 6: Doppler signatures of local multipath signals for the case of stable ionosphere while the target is moving towards the radar at altitude $h = 20$ km with velocity $\dot{R}_0 = -400$ m/s and acceleration $\ddot{R} = -3$ m/s². (a) Simulated Doppler signature; (b) Spectrogram using a Hamming window of size 256; (c) Fractional Fourier transform; (d) Peak detection in frequency domain and the corresponding α plotted for each of the peak frequencies. The input SNR is set at -15 dB. The target parameters estimated from this simulation are $\hat{h} = 16.82$ km, $\hat{R}_0 = -400.84$ m/s, and $\hat{\ddot{R}} = -2.998$ m/s².

obtain

$$\hat{h} = \frac{\Delta f_{D,0}(R_0^2 - 2H_0^2)}{2H_0 \left(\frac{8H_0\dot{H}_0 f_c}{cR_0} + \bar{f}_{D,0} \right) - \frac{(R_0^2 - 2H_0^2)}{2H_0} \bar{f}_{D,0}^{\text{clutter}}}, \quad (35)$$

which explicitly shows the dependence of \hat{h} on both the average Doppler frequency, \bar{f}_D , and the difference Doppler frequency, Δf_D .

V. TARGET RESOLVABILITY

It can be observed from Fig. 1 that each target results in three distinct Doppler components due to three distinct round-trip paths. In the previous sections, we noted that the Doppler frequency estimation for signals corresponding to all three paths is important to resolve the altitude information of the target. If the three Doppler components are closely spaced, i.e., $|\Delta f_D|$ is very small, it becomes challenging to resolve the three distinct Doppler components. In the following, we examine the resolvability conditions of the three Doppler components with respect to the target velocity and the ionosphere velocity for a fixed CPI.

Fig. 2 depicts the difference Doppler component Δf_D against a range of target and ionosphere velocities under the condition $R = 2,500$ km, $H = 350$ km, and $f_c = 16$ MHz. Considering the 60-second CPI assumed in this paper with a

moderate window effect, we bound the region of $|\Delta f_D| < 0.02$ Hz by red lines as the likely region where the Doppler frequencies are difficult to resolve, resulting in challenging target geo-location. The gray level demonstrates the amplitude of Δf_D , i.e., dark black color shows high resolvability whereas white region shows challenging resolvability of the Doppler signatures. It is observed in Fig. 2 that the values of $|\Delta f_D|$ for the most part remain significant such that the three Doppler components are resolvable, thus resulting in favorable target geo-location capability.

In order to illustrate the impact of Δf_D on the frequency estimation performance, we present the root mean square error (RMSE) of the multipath Doppler frequency estimates with respect to varying Δf_D and input SNR in Fig. 3. The RMSE results are obtained by assuming that the chirp rates are correctly estimated through FrFT. The RMSE is calculated using the following equation:

$$\text{RMSE} = \sqrt{\frac{1}{3M} \sum_{m=1}^M \sum_{i=1}^3 \left(f_{D,i}^{\text{centroid}} - \bar{f}_{D,i}^{\text{centroid}} \right)^2}, \quad (36)$$

where $\bar{f}_{D,i}^{\text{centroid}}$ is the estimated centroid Doppler frequency corresponding to the actual centroid Doppler frequency $f_{D,i}^{\text{centroid}}$ of the i th propagation path and M is the total number of trials. We observe in Fig. 3 that the RMSE of the estimated multipath Doppler frequencies is low when $|\Delta f_D|$ is higher

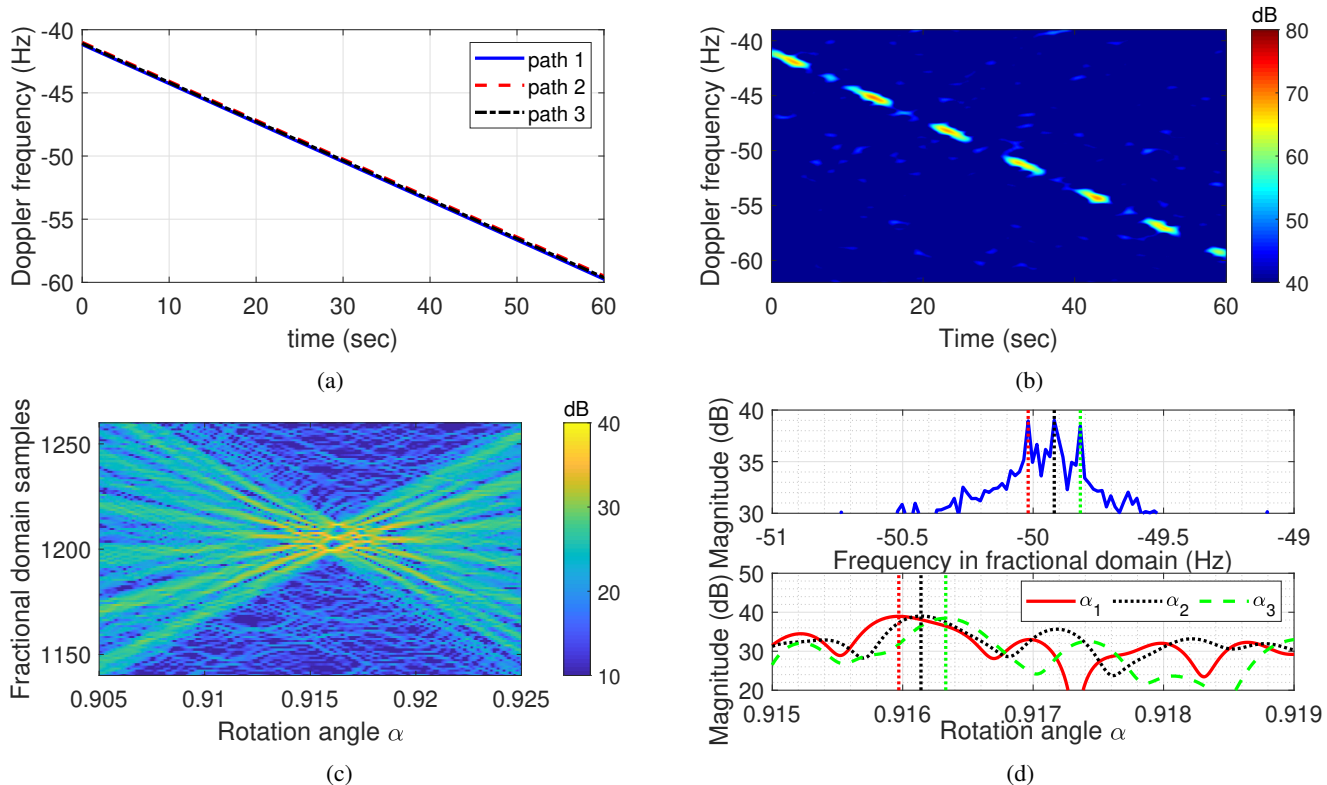


Fig. 7: Doppler signatures of local multipath signals for the case of stable ionosphere while the target is moving away from the radar at altitude $h = 20$ km with velocity $\dot{R}_0 = 400$ m/s and acceleration $\ddot{R} = 3$ m/s². (a) Simulated Doppler signature; (b) Spectrogram; (c) Fractional Fourier transform; (d) Peak detection in frequency domain and the corresponding α plotted for each of the peak frequencies. The input SNR is set at -15 dB. The target parameters estimated from this simulation are $\hat{h} = 17.25$ km, $\hat{R}_0 = 400.86$ m/s, and $\hat{\ddot{R}} = 3.015$ m/s².

than 0.02 Hz, provided that the input SNR is reasonably high. On the other hand, it becomes difficult to extract reliable frequency estimates when $|\Delta f_D| \leq 0.02$ Hz due to the close spectral proximity of the three multipath Doppler signatures. This observation supports the analysis in Fig. 2 where the challenging frequency resolution situations are bounded by the two red lines. Note that the results depend primarily on the value of Δf_D , which is a joint function of both target and ionosphere parameters. For a specific value of Δf_D , the results are insensitive to the instantaneous target and ionosphere velocities.

VI. SIMULATION RESULTS

In this section, we provide simulation results for different scenarios of ionosphere and target motions and show results of the joint estimation of ionosphere and target parameters. We consider the flat-earth model and the parameters for simulations are listed in Table I unless otherwise specified.

A. Case A: Stable Ionosphere

In this subsection, we consider the case that the ionosphere layer is stable with a constant height. Two examples are considered where the target respectively has a constant velocity and has a constant acceleration.

1) *Constant Target Velocity*: In the first simulation, we consider a baseline case where the ionosphere layer remains stationary at the height of $H = 350$ km above the earth with $\dot{H}_0 = 0$ m/s and $\ddot{H} = 0$ m/s², and the target is moving towards the radar with a constant speed of $\dot{R}_0 = -400$ m/s, and the target acceleration \ddot{R} is 0 m/s². Note that the minus sign in the target speed implies the decrease of target range over time. Fig. 4(a) shows the simulated Doppler signatures which clearly exhibit the three frequency components corresponding to the different multipath signals. Fig. 4(b) shows the spectrogram of the three Doppler signatures using a Hamming window of length 4096 samples (which approximately amounts to 29.3 s). Since the target acceleration is zero, the chirp rates obtained from Eq. (13) is zero for all three Doppler components. The actual chirp rate estimated from the Doppler signatures is -4.85×10^{-4} Hz/s for all three components. Such a small chirp rate is due to the change in the range that alters the observation direction. Thus, the three Doppler components can be treated as three parallel horizontal lines (sinusoids) with a constant Doppler frequency difference Δf_D and a zero chirp rate. The FrFT result of the received signal depicted in Fig. 4(c) clearly shows that the rotation angle α_{opt} is approximately 1 for all three Doppler components, implying zero chirp rates.

Fig. 4(d) provides two plots to show the rotation angles and corresponding frequencies more clearly. In the upper panel of Fig. 4(d), the maximum magnitude of the FrFT

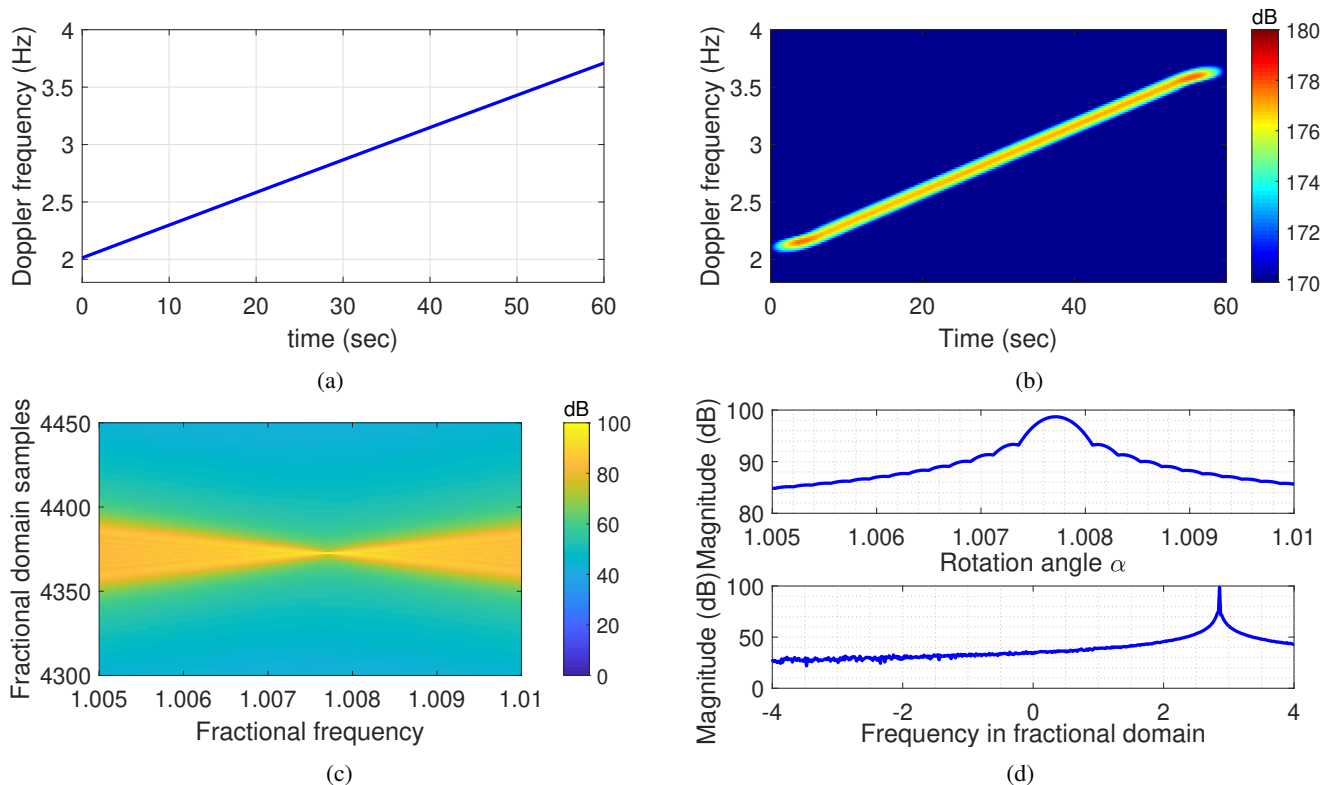


Fig. 8: Doppler signatures of the clutter for the dynamic ionosphere case where ionosphere is moving towards the sea with initial velocity $\dot{H}_0 = -35$ m/s and constant acceleration of $\ddot{H} = -0.5$ m/s²: (a) Simulated Doppler signature; (b) Spectrogram using a Hamming window of size 1024; (c) Fractional Fourier transform; (d) Peak detection in rotation angle α and frequency domains. Clutter-to-noise ratio is set at 35 dB. The ionosphere parameters estimated from this simulation are $\hat{H}_0 = -33.65$ m/s, and $\hat{\ddot{H}} = -0.48$ m/s².

is depicted with respect to the frequency in the fractional domain. In the lower panel of Fig. 4(d), on the other hand, we show the magnitude spectrum of the FrFT corresponding to the rotation angle. Since the CPI is 60 seconds, the FrFT provides us the estimate of frequencies at the midpoint of the CPI, i.e., at $T/2 = 30$ s. As the chirp rate is zero, the individual frequencies of the three Doppler components can be considered constant throughout the CPI, and the three Doppler components are estimated to be 40.97 Hz, 41.07 Hz, and 41.15 Hz, whereas the actual Doppler frequencies are 41.00 Hz, 41.09 Hz and 41.17 Hz, respectively. The estimated chirp rate was approximately -6.6×10^{-4} Hz/s for the three Doppler components. Using Eq. (18), we calculate the target altitude, initial velocity, and the acceleration to be 18.81 km, -400.48 m/s, and -4.6×10^{-5} m/s², respectively.

In the second simulation, all the parameters remain the same, except that the target is now moving away from the radar with a velocity of $R = 400$ m/s. Fig. 5 shows similar results for the frequency and chirp rate estimation. The target parameters of the altitude, initial velocity, and the acceleration are estimated to be 17.73 km, 401.13 m/s, and -1.5×10^{-5} m/s².

2) *Constant Target Acceleration:* For the third simulation, the target is assumed to be moving with an initial velocity of $\dot{R}_0 = -400$ m/s towards the radar and an acceleration of $\ddot{R} = -3$ m/s². The ionosphere is assumed to be stable

at an altitude of 350 km. Fig. 6(a) shows the three actual Doppler components generated by the motion of the target. As the target motion involves acceleration in this case, the three chirps have a high chirp rate which is in accordance with Eq. (13). It can be observed in Fig. 6(b) that it is difficult to resolve the three Doppler components in the spectrogram even with a small window size of 256 samples. However, these three components can be clearly resolved by using the FfFT, as shown in Fig. 6(c). Moreover, Fig. 6(d) illustrates the FrFT magnitude with respect to the frequency in the fractional domain and to the rotation angle, respectively. It is observed that the three frequency peaks emerge at 49.76 Hz, 49.86 Hz, and 49.96 Hz in the fractional domains and their respective rotation angles result in the chirp rates of 0.306558 Hz/s, 0.307241 Hz/s, and 0.307925 Hz/s, respectively. Using Eq. (17), the estimated frequencies at the midpoint of the CPI become 50.20 Hz, 50.30 Hz, and 50.40 Hz, respectively. Incorporating these estimated chirp rates, we can estimate the initial Doppler frequencies at time 0 s to be 41.00 Hz, 41.09 Hz, 41.17 Hz, respectively, which well match the corresponding actual Doppler frequencies 41.00 Hz, 41.09 Hz, and 41.17 Hz. Further, by using Eq. (18), we calculate the target altitude, initial velocity, and the acceleration to be 16.82 km, -400.84 m/s, and -2.998 m/s², respectively.

In the fourth simulation, we keep all the parameters except that the target is now moving away from the radar with an

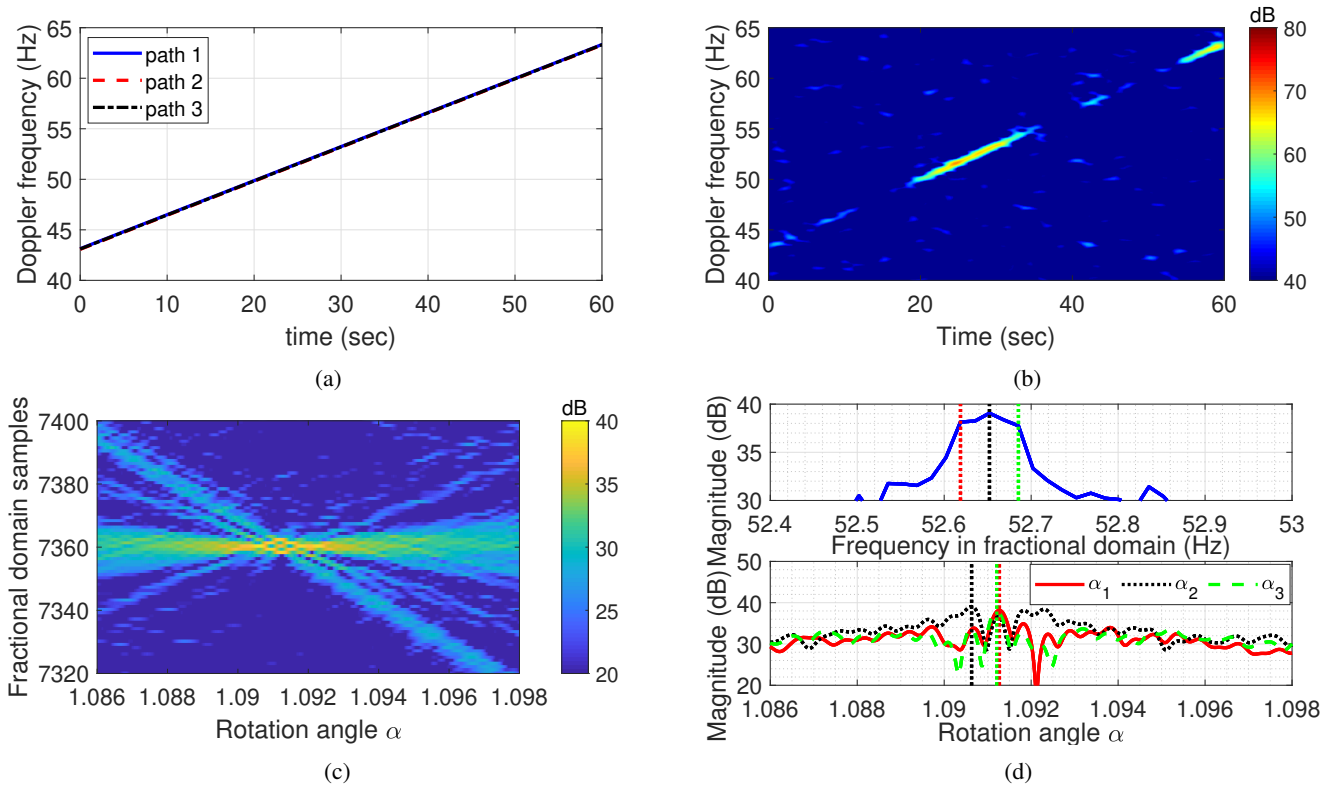


Fig. 9: Doppler signatures of local multipath signals for the case of dynamic ionosphere moving towards the sea with initial velocity $\dot{H}_0 = -35$ m/s and acceleration $\ddot{H} = -0.5$ m/s². The target is moving towards the radar at altitude $h = 20$ km with velocity $\dot{R}_0 = -400$ m/s and acceleration $\ddot{R} = -3$ m/s². (a) Simulated Doppler signature; (b) Spectrogram using a Hamming window of size 256; (c) Fractional Fourier transform; (d) Peak detection in frequency domain and the corresponding α plotted for each of the peak frequencies. Input SNR was set at -15 dB. The target parameters estimated from this simulation are $\hat{h} = 19.66$ km, $\hat{R}_0 = -400.86$ m/s, and $\hat{\ddot{R}} = -3.27$ m/s².

initial velocity of $\dot{R} = 400$ m/s and an acceleration of 3 m/s². Similar estimation results for the frequency and chirp rate are observed in Fig. 7. By using Eq. (18), the target parameters of altitude, initial velocity, and the acceleration are estimated as 17.25 km, 400.86 m/s, and 3.015 m/s², respectively.

B. Case B: Dynamic Ionosphere

In this subsection, we examine the joint ionosphere and moving target parameter estimation for the case of dynamic ionosphere where the ionosphere height varies with a constant acceleration. Both ascending and descending ionosphere layer cases are considered. We first discuss the ionosphere parameter estimation based on clutter Doppler signature, and the target parameter estimation is then discussed.

1) *Ionosphere Parameter Estimation*: First, we assume that the ionosphere is moving downwards with an initial velocity of $\dot{H}_0 = -35$ m/s and an acceleration of $\ddot{H} = -0.5$ m/s². Fig. 8(a) shows the actual Doppler signature of the clutter generated due to the ionosphere motion, and Fig. 8(b) illustrates the corresponding spectrogram. For the parameters being considered, the clutter frequency component is much closer to the zero Doppler frequency compared to the target Doppler frequencies so that they can be easily separated in the time-frequency or fractional Fourier domain. Fig. 8(c) shows the FrFFT result of the clutter Doppler component whereas

Fig. 8(d) shows the respective peaks in frequency and rotation angle domains. The rotational angle was estimated to be at 1.007710 , yielding an estimated chirp rate of 0.028257 Hz/s which is very close to the actual chirp rate of 0.028261 Hz/s. Using this estimated chirp rate and the estimated centroid Doppler frequency at 30 sec, we calculate the estimated f_D^{clutter} at 0 sec and 60 sec to be 2.01 Hz and 3.70 Hz, respectively, which exactly match the actual values of the clutter Doppler frequency. We exploit Eq. (24) and (25) to estimate the initial velocity and acceleration of the ionosphere to be -33.65 m/s and -0.47 m/s², respectively. The approximated Eq. (26) provides the ionosphere acceleration of -0.45 m/s² which is also close to the actual ionosphere acceleration.

Next, we change the direction of the ionosphere motion to move upwards with an initial velocity of 35 m/s and an acceleration of 0.5 m/sec², and similar results are obtained. The initial velocity and acceleration are estimated as 33.9 m/s and 0.48 m/s², respectively. These results match well with the actual values.

2) *Target Parameter Estimation*: Now, we consider the target parameter estimation for the dynamic ionosphere case. We first consider that the ionosphere is moving downwards with an initial velocity $\dot{H}_0 = -35$ m/s and an acceleration of $\ddot{H} = -0.5$ m/s². The target moves towards the radar such that its initial velocity is $\dot{R}_0 = -400$ m/s and the acceleration

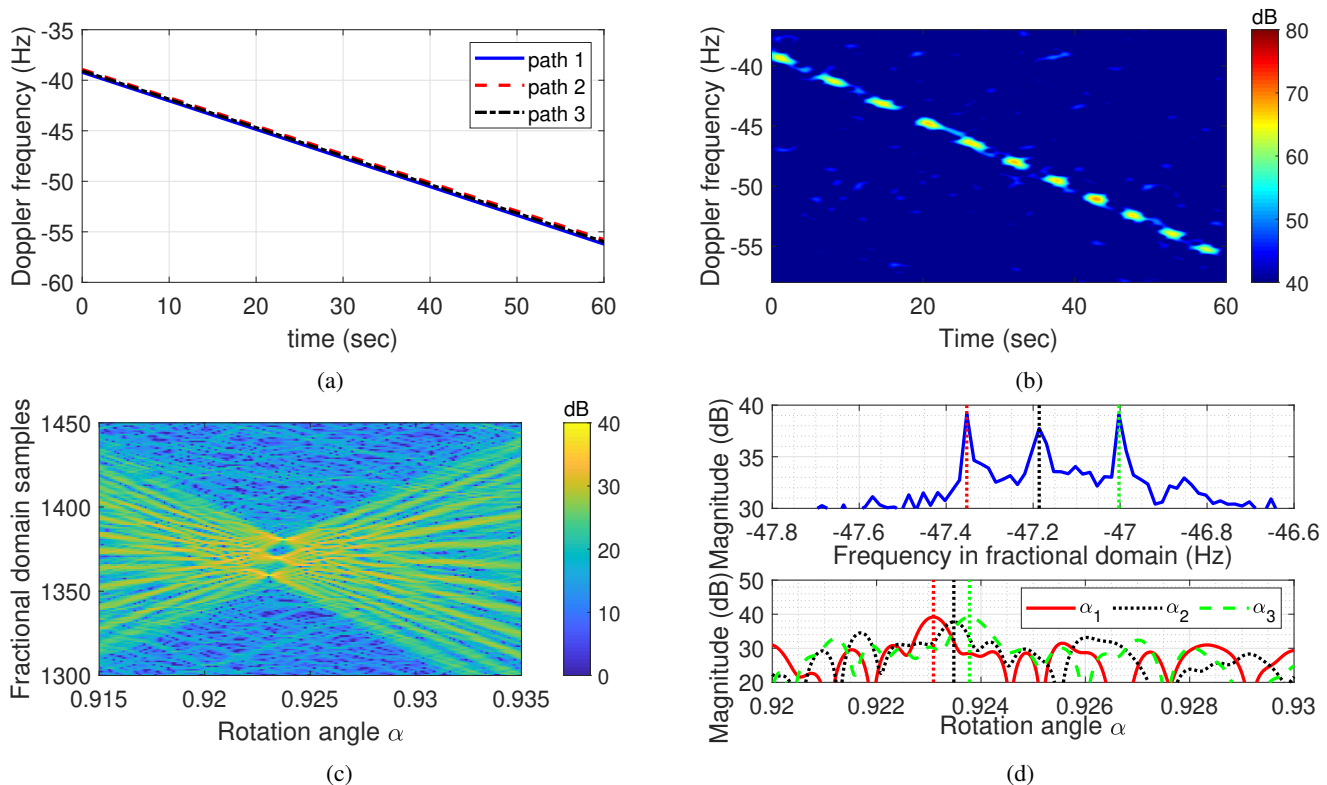


Fig. 10: Doppler signatures of local multipath signals for the case of dynamic ionosphere moving towards the sea with initial velocity $\dot{H}_0 = -35$ m/s and acceleration $\ddot{H} = -0.5$ m/s². The target is moving away from the radar at altitude $h = 20$ km with velocity $\dot{R}_0 = 400$ m/s and acceleration $\ddot{R} = -3$ m/s². (a) Simulated Doppler signature; (b) Spectrogram using a Hamming window of size 256; (c) Fractional Fourier transform; (d) Peak detection in frequency domain and the corresponding α plotted for each of the peak frequencies. Input SNR was set at -15 dB. The target parameters estimated from this simulation are $\hat{h} = 18.41$ km, $\hat{R}_0 = 400.75$ m/s, and $\hat{\ddot{R}} = 2.74$ m/s².

is $\ddot{R} = -3$ m/s. Fig. 9 shows the results for this case. The peak frequencies observed in the fractional domain are 52.61 Hz, 52.65 Hz, and 52.68 Hz, respectively, which are mapped to the estimated centroid frequencies of 53.16 Hz, 53.19 Hz, and 53.23 Hz, respectively. The estimated target altitude, initial velocity and acceleration are then calculated as 19.66 km, -400.96 m/s, and -3.27 m/s². Similarly, Fig. 10 illustrates the parameter estimation results for the case that the target moves away from the radar with an initial speed of 400 m/s and acceleration of 3 m/s², whereas the ionosphere motion parameters remain the same. The target altitude, initial velocity, and acceleration are estimated for this case to be 18.41 km, 400.75 m/s, and 2.744 m/s², respectively.

Next, we consider the case that the ionosphere layer ascends with an initial velocity of $\dot{H}_0 = 35$ m/s and an acceleration of $\ddot{H} = 0.5$ m/s². The target moves towards the radar with an initial velocity of $\dot{R}_0 = -400$ m/s and acceleration of $\ddot{R} = -3$ m/s². The simulation results for this case are depicted in Fig. 11. The peak frequencies in the fractional domain are 46.86 Hz, 47.05 Hz, and 47.23 Hz, respectively, and the corresponding centroid frequencies are estimated to be 47.19 Hz, 47.38 Hz, and 47.56 Hz. The target altitude, initial velocity and acceleration are estimated to be 19.86 km, -400.97 m/s, and -2.70 m/s², respectively. Similarly, Fig. 12 depicts the parameter estimation results for the case of that the target

moves away from the radar with an initial speed of 400 m/s and acceleration of 3 m/s², whereas the ionosphere motion parameters remain the same. In this case, the target altitude, initial velocity, and acceleration are estimated to be 17.67 km, 400.95 m/s, and 2.744 m/s², respectively.

In this paper, we presented the mathematical formulations and simulation results for parameter estimation of a single target. In the presence of multiple targets, the proposed method can be readily employed if the targets are separable in the range, Doppler, and angular domains.

VII. CONCLUSION

In this paper, we have addressed the joint estimation of target and ionosphere parameters in OTHR by exploiting the local multipath signal model. We assumed a constant altitude for the target, which flies towards or away from the radar with a constant acceleration, whereas the ionosphere height may remain constant or changes with a constant acceleration. It was observed that the Doppler signatures of the target and ionosphere motion can be characterized as parallel chirps. Under practically valid assumptions, analytical expressions were derived for the estimation of velocity and acceleration of the ionosphere and provide insightful observations of the determining parameters. Moreover, the expressions for

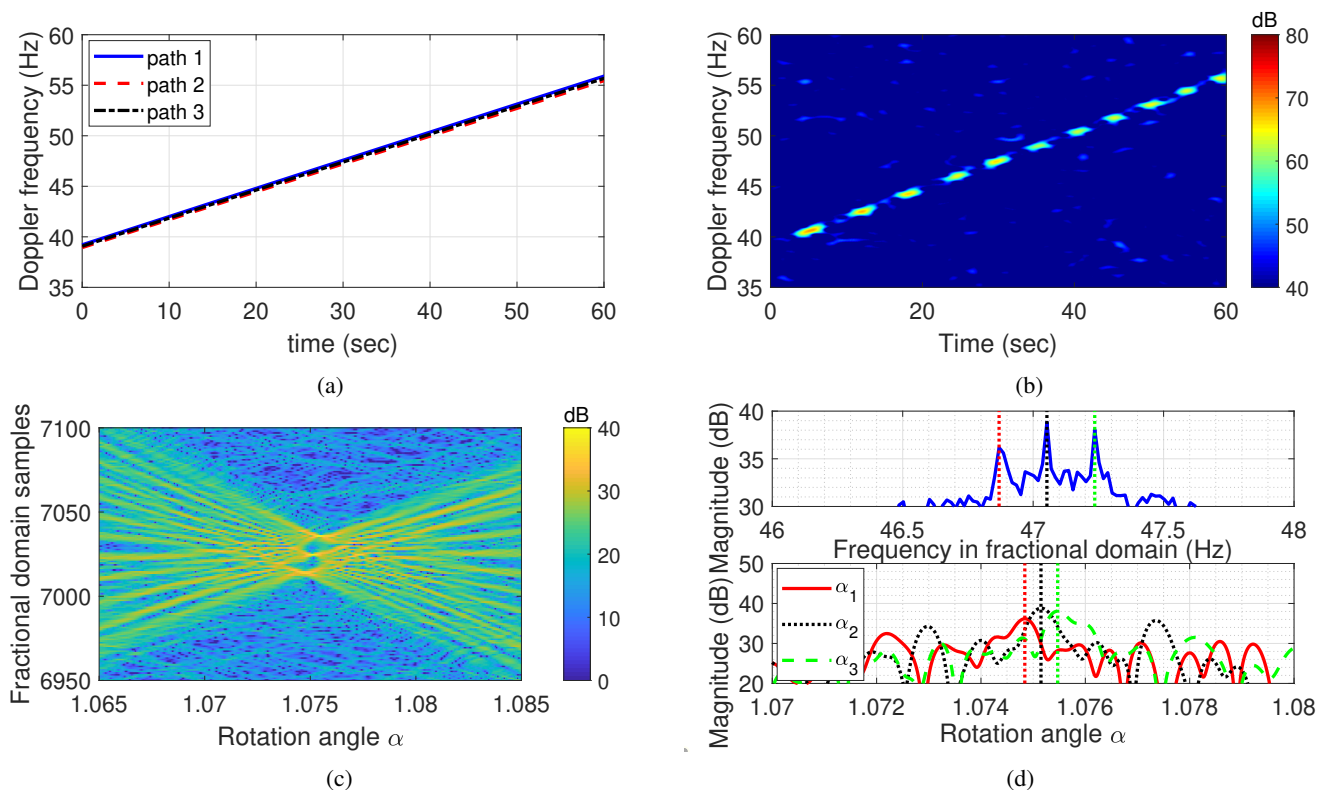


Fig. 11: Doppler signatures of local multipath signals for the case of dynamic ionosphere moving towards the sky with initial velocity $\dot{H}_0 = 35$ m/s and acceleration $\ddot{H} = 0.5$ m/s². The target is moving towards the radar at altitude $h = 20$ km with velocity $\dot{R}_0 = -400$ m/s and acceleration $\ddot{R} = -3$ m/s². (a) Simulated Doppler signature; (b) Spectrogram using a Hamming window of size 256; (c) Fractional Fourier transform; (d) Peak detection in frequency domain and the corresponding α plotted for each of the peak frequencies. Input SNR was set at -15 dB. The target parameters estimated from this simulation are $\hat{h} = 19.86$ km, $\hat{R}_0 = -400.97$ m/s, and $\hat{R} = -2.71$ m/s².

the target altitude, velocity and acceleration have also been presented for the case of stable as well as dynamic ionosphere conditions based on the resolved Doppler signatures generated by both the target and the ionosphere. Simulation results demonstrate the effectiveness of the proposed method to estimate these parameters based on a short period of processing time.

REFERENCES

- [1] M. Headrick and M. I. Skolnik, "Over-the-horizon radar in the HF band," *Proc. IEEE*, vol. 62, no. 6, pp. 664–673, 1974.
- [2] L. F. McNamara, *The Ionosphere: Communications, Surveillance, and Direction Finding*, Krieger Publishing Company, 1999.
- [3] J. M. Headrick and S. J. Anderson, "HF over-the-horizon radar," Chapter 20 in M. Skolnik (ed.), *Radar Handbook, 3rd Ed.* McGraw-Hill, 2008.
- [4] G. A. Fabrizio, *High Frequency Over-the-Horizon Radar: Fundamental Principles, Signal Processing, and Practical Applications*. McGraw-Hill, 2013.
- [5] K. Bell, "MAP-PF multi-mode tracking for over-the-horizon radar," in *Proc. IEEE Radar Conf.*, Atlanta, GA, May 2012, pp. 326–331.
- [6] Y. Zhang, M. G. Amin, and G. J. Frazer, "High-resolution time–frequency distributions for manoeuvring target detection in over-the-horizon radars," *IEE Proc.-Radar Sonar Navig.*, vol. 150, no. 4, pp. 299–304, 2003.
- [7] H. Su, H. Liu, P. Shui, and Z. Bao, "Adaptive beamforming for nonstationary HF interference cancellation in skywave over-the-horizon radar," *IEEE Trans. Aerospace Electron. Syst.*, vol. 49, no. 1, pp. 312–324, Jan. 2013.
- [8] K. Lu, and X. Liu, "Enhanced visibility of maneuvering targets for high-frequency over-the-horizon radar," *IEEE Trans. Antennas Propag.*, vol. 53, no. 1, pp. 404–411, Jan. 2005.
- [9] J. Hu, M. Li, Q. He, Z. He, and R. S. Blum, "Joint estimation of MIMO-OTH radar measurements and ionospheric parameters," *IEEE Trans. Aerospace Electron. Syst.*, vol. 53, no. 6, pp. 2789–2805, 2017.
- [10] E. Lyon, and K. L. Kodan, "Target altitude estimation and noncooperative type classification in OTH radar," *SRI Int. Final Sci. Tech. Rep.*, June 1996.
- [11] M. Papazoglou and J. L. Krolik, "Matched-field estimation of aircraft altitude from multiple over-the-horizon radar revisits," *IEEE Trans. Signal Process.*, vol. 47, no. 4, pp. 966–976, April 1999.
- [12] M. Papazoglou and J. L. Krolik, "Estimation of aircraft altitude and altitude rate with over-the-horizon radar," in *Proc. IEEE Int. Conf. Acoust. Speech Signal Process.*, Phoenix, AZ, March 1999, pp. 2103–2106.
- [13] R. H. Anderson, S. Kraut, and J. L. Krolik, "Robust altitude estimation for over-the-horizon radar using a state-space multipath fading model," *IEEE Trans. Aerospace Electron. Syst.*, vol. 39, no. 1, pp. 192–201, 2003.
- [14] Y. D. Zhang, J. J. Zhang, M. G. Amin, and B. Himed, "Instantaneous altitude estimation of maneuvering targets in over-the-horizon radar exploiting multipath Doppler signatures," *EURASIP J. Adv. Signal Process.*, vol. 2013, no. 2013:100, pp. 1–13, May 2013.
- [15] Z. Luo, Z. He, X. Chen, and K. Lu, "Target location and height estimation via multipath signal and 2D array for sky-wave over-the-horizon radar," *IEEE Trans. Aerospace Electron. Syst.*, vol. 52, no. 2, pp. 617–631, April 2016.
- [16] J. Praschifka, L. J. Durbridge and J. Lane, "Investigation of target altitude estimation in skywave OTH radar using a high-resolution ionospheric sounder," in *Proc. Intl. Radar Conf.*, Bordeaux, France, Oct. 2009, pp. 1–6.

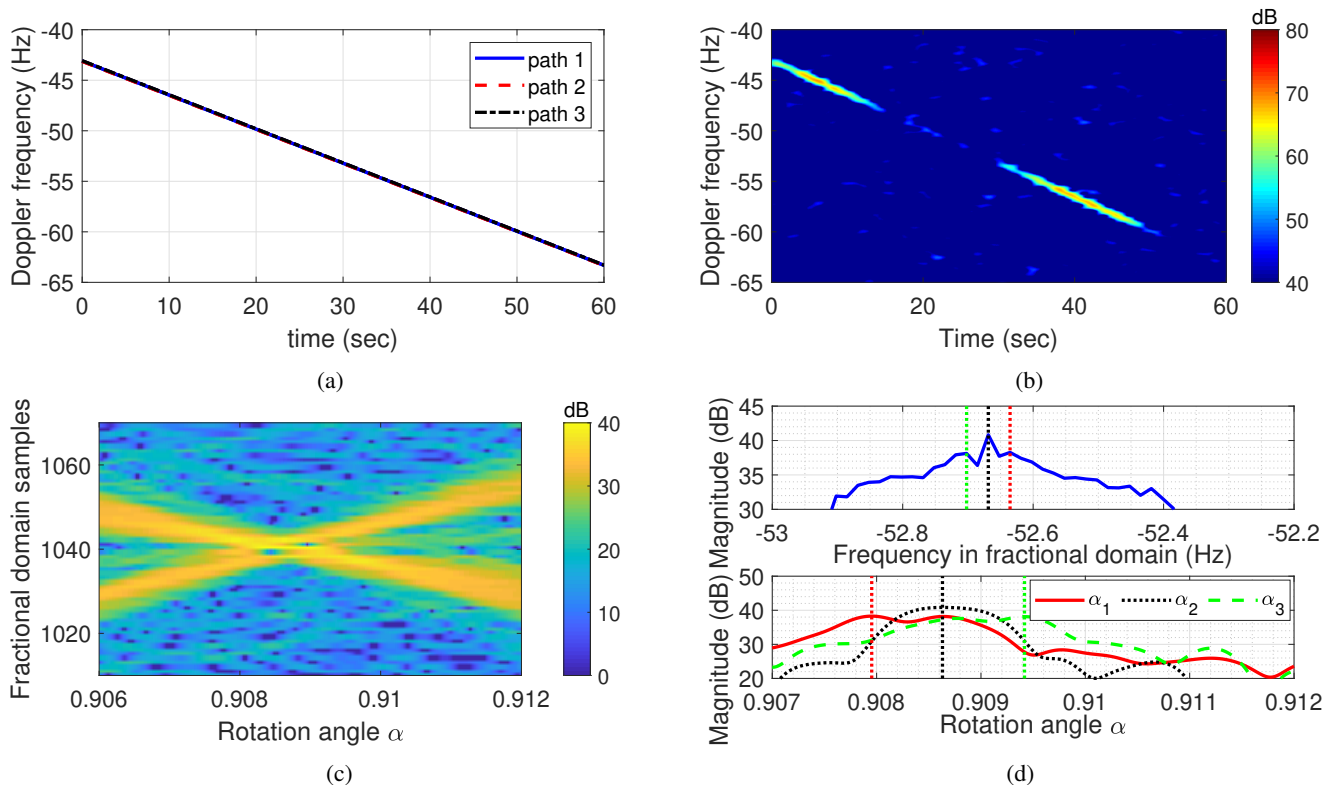


Fig. 12: Doppler signatures of local multipath signals for the case of dynamic ionosphere moving towards the sky with initial velocity $\dot{H}_0 = 35$ m/s and acceleration $\ddot{H} = 0.5$ m/s. The target is moving away from the radar at altitude $h = 20$ km with velocity $\dot{R}_0 = 400$ m/s and acceleration $\ddot{R} = 3$ m/s². (a) Simulated Doppler signature; (b) Spectrogram using a Hamming window of size 256; (c) Fractional Fourier transform; (d) Peak detection in frequency domain and the corresponding α plotted for each of the peak frequencies. Input SNR was set at -15 dB. The target parameters estimated from this simulation are $\hat{h} = 17.67$ km, $\hat{R}_0 = 400.95$ m/s, and $\hat{R} = 3.29$ m/s².

- [17] Y. D. Zhang, M. G. Amin, and B. Himed, "Altitude estimation of maneuvering targets in MIMO over-the-horizon radar," in *Proc. IEEE Sensor Array and Multichannel Signal Process. Workshop*, Hoboken, NJ, 2012, pp. 257–260.
- [18] C. Ioana, M. G. Amin, Y. D. Zhang, and F. Ahmad, "Characterization of Doppler effects in the context of over-the-horizon radar," in *Proc. IEEE Radar Conf.*, Washington, D.C., 2010, pp. 506–510.
- [19] C. Ioana, Y. D. Zhang, M. G. Amin, F. Ahmad, G. Frazer, and B. Himed, "Time-frequency characterization of micro-multipath signals in over-the-horizon radar," in *Proc. IEEE Radar Conf.*, Atlanta, GA, 2012, pp. 671–675.
- [20] Y. D. Zhang and B. Himed, "Multipath Doppler difference estimation in over-the-horizon radar," in *Proc. IEEE Radar Conf.*, Oklahoma City, OK, April 2018.
- [21] F. Bertoni, I. S. Batista, M. A. Abdu, B. W. Reinisch, and E. A. Kherani, "A comparison of ionospheric vertical drift velocities measured by Digisonde and incoherent scatter radar at the magnetic equator," *J. Atmos. Sol.-Terr. Phys.*, vol. 68, no. 6, pp. 669–678, Mar. 2006.
- [22] G. S. Sales, *High Frequency (HF) Radiowave Propagation*. University of Massachusetts Lowell Scientific Report, No. PL-TR-92-2123, April 1992.
- [23] C. Hou, Y. Wang, and J. Chen, "Estimating target heights based on the earth curvature model and micromultipath effect in skywave OTH radar," *J. Applied Math.*, vol. 2014, article ID 424191, pp. 1–14, 2014.
- [24] J. Xu, J. Yu, Y. Peng, and X. Xia, "Radon-Fourier Transform for radar target detection, I: Generalized Doppler filter bank," *IEEE Trans. Aerosp. Electron. Syst.*, vol. 47, no. 2, pp. 1186–1202, Apr. 2011.
- [25] X. Chen, J. Guan, N. Liu, and Y. He, "Maneuvering target detection via Radon-Fractional Fourier Transform-based long-time coherent integration," *IEEE Trans. Signal Process.*, vol. 62, no. 4, pp. 939–953, Feb. 2014.
- [26] H. Zhang, G. Bi, W. Yang, S. G. Razul, and C. M. S. See, "IF estimation of FM signals based on time-frequency image," *IEEE Trans. Aerospace Electron. Syst.*, vol. 51, no. 1, pp. 326–343, Jan. 2015.
- [27] T.-Z. Xu, B.-Z. Li, *Linear Canonical Transform and its Applications*, SciencePress, Beijing, China, 2013.
- [28] H. M. Ozaktas, M. A. Kutay, and Z. Zalevsky, *The Fractional Fourier Transform: With Applications in Optics and Signal Processing*. Wiley, 2001.
- [29] E. Sejdić, I. Djurović, and L. Stanković, "Fractional Fourier transform as a signal processing tool: An overview of recent developments," *Signal Process.*, vol. 91, no. 6, pp. 1351–1369, June 2011.
- [30] H.-B. Sun, G.-S. Liu, H. Gu, and W.-M. Su, "Application of the fractional Fourier transform to moving target detection in airborne SAR," *IEEE Trans. Aerosp. Electron. Syst.*, vol. 38, no. 4, pp. 1416–1424, Oct. 2002.



Ammar Ahmed (Member, IEEE) received Ph.D. degree from Temple University, Philadelphia, USA, in 2021.

Dr. Ahmed is currently a Radar Signal Processing Engineer at Aptiv, Agoura Hills, CA, USA. His research interests are in signal processing, optimization, machine learning, and radar systems. He served as a Program Co-Chair for the 2021 IEEE Signal Processing in Medicine and Biology Symposium and is a General Co-Chair for the 2022 IEEE Signal Processing in Medicine and Biology Symposium.



Yimin D. Zhang (Fellow, IEEE) received the Ph.D. degree from the University of Tsukuba, Tsukuba, Japan, in 1988.

He is currently an Associate Professor with the Department of Electrical and Computer Engineering, Temple University, Philadelphia, PA, USA. From 1998 to 2015, he was a Research Faculty with the Center for Advanced Communications, Villanova University, Villanova, PA, USA. His research interests include array signal processing, compressive sensing, machine learning, convex optimization, and time-frequency analysis with applications to radar, wireless communications, and satellite navigation. Dr. Zhang is an Associate Editor for *IEEE Transactions on Aerospace and Electronic Systems* and for *Signal Processing*. He was an Associate Editor for *IEEE Transactions on Signal Processing*, *IEEE Signal Processing Letters*, and *Journal of the Franklin Institute*. He was a Technical Co-Chair of the 2018 IEEE Sensor Array and Multichannel Signal Processing Workshop. He was the recipient of the 2016 IET Radar, Sonar & Navigation Premium Award, the 2017 IEEE Aerospace and Electronic Systems Society Harry Rowe Mimno Award, the 2019 IET Communications Premium Award, and the 2021 EURASIP Best Paper Award for Signal Processing. He coauthored two papers that respectively received the 2018 and 2021 IEEE Signal Processing Society Young Author Best Paper Awards. He is a Fellow of SPIE.



Braham Himed (Fellow, IEEE) received the Engineer degree in electrical engineering from the Ecole Nationale Polytechnique of Algiers, in 1984, and the M.S. and Ph.D. degrees in electrical engineering from Syracuse University in 1987 and 1990, respectively. He is currently a Division Research Fellow with the Air Force Research Laboratory, Sensors Directorate, Distributed RF Sensing Branch, Dayton, OH, where he is involved with several aspects of radar developments. His research interests include detection, estimation, multichannel adaptive

signal processing, time series analyses, array processing, adaptive processing, waveform diversity, MIMO radar, passive radar, and over the horizon radar. He is also a Fellow of AFRL (Class of 2013). He was a recipient of the 2001 IEEE region I award for his work on bistatic radar systems, algorithm development, and phenomenology. He was also the recipient of the 2012 IEEE Warren White award for excellence in radar engineering. He is also a past Chair of the AESS Radar Systems Panel, and a member of the AESS Board of Governors (2021–2023).